

# Search for in-band transitions in the candidate superdeformed band in $^{28}\text{Si}$

L. Morris,<sup>1</sup> D. G. Jenkins,<sup>1,2,\*</sup> M. N. Harakeh,<sup>3,4</sup> J. Isaak,<sup>5,3</sup> N. Kobayashi,<sup>3</sup> A. Tamii,<sup>3</sup> S. Adachi,<sup>3</sup> P. Adsley,<sup>6</sup> N. Aoi,<sup>3</sup> A. Bracco,<sup>7,8</sup> A. Brown,<sup>1</sup> M. P. Carpenter,<sup>9</sup> J. J. Carroll,<sup>10</sup> S. Courtin,<sup>2,11</sup> F. C. L. Crespi,<sup>7,8</sup> P. J. Davies,<sup>1</sup> G. Fruet,<sup>11</sup> Y. D. Fang,<sup>3</sup> H. Fujita,<sup>3</sup> G. Gey,<sup>3</sup> T. H. Hoang,<sup>3</sup> N. Ichige,<sup>12</sup> E. Ideguchi,<sup>3</sup> A. Inoue,<sup>3</sup> C. Iwamoto,<sup>13</sup> T. Koike,<sup>12</sup> M. Kumar Raju,<sup>3</sup> M. L. Liu,<sup>14</sup> D. Montanari,<sup>2,11</sup> P. von Neumann-Cosel,<sup>5</sup> S. Noji,<sup>15</sup> H. J. Ong,<sup>3,†</sup> D. Savran,<sup>16</sup> J. M. Schmitt,<sup>15</sup> C. Sullivan,<sup>15</sup> B. Wasilewska,<sup>17</sup> M. Weinert,<sup>18</sup> V. Werner,<sup>5</sup> Y. Yamamoto,<sup>3</sup> R. G. T. Zegers,<sup>15</sup> X. H. Zhou,<sup>14</sup> and S. Zhu<sup>9</sup>

<sup>1</sup>*Department of Physics, University of York, Heslington, York, YO10 5DD, United Kingdom*

<sup>2</sup>*USIAS, University of Strasbourg, Strasbourg F-67083, France*

<sup>3</sup>*RCNP, Osaka University, Ibaraki, Osaka 5670047, Japan*

<sup>4</sup>*Nuclear Energy group, ESRIG, University of Groningen, 9747 AA Groningen, The Netherlands*

<sup>5</sup>*Institut für Kernphysik, Technische Universität Darmstadt, 64289 Darmstadt, Germany*

<sup>6</sup>*iThemba Laboratory for Accelerator Based Sciences, Somerset West 7129, South Africa*

<sup>7</sup>*Dipartimento di Fisica dell'Università degli Studi di Milano, I-20133 Milano, Italy*

<sup>8</sup>*INFN, Sezione di Milano, I-20133 Milano, Italy*

<sup>9</sup>*Physics Division, Argonne National Laboratory, Argonne, Illinois 60439, USA*

<sup>10</sup>*DEVCOM/Army Research Laboratory, Adelphi, Maryland 20783, USA*

<sup>11</sup>*IPHC, Université de Strasbourg, Strasbourg F-67037, France*

<sup>12</sup>*Department of Physics, Tohoku University, Sendai 980-8578, Japan*

<sup>13</sup>*Center for Nuclear Study (CNS), University of Tokyo, Bunkyo, Tokyo 113-0033, Japan*

<sup>14</sup>*Institute of Modern Physics, Chinese Academy of Sciences, Lanzhou 730000, China*

<sup>15</sup>*National Superconducting Cyclotron Laboratory,*

*Michigan State University, East Lansing, Michigan 48824-1321, USA*

<sup>16</sup>*GSI Helmholtzzentrum für Schwerionenforschung GmbH, 64291 Darmstadt, Germany*

<sup>17</sup>*Institute of Nuclear Physics, PAN, 31-342 Kraków, Poland*

<sup>18</sup>*University of Cologne, Institute for Nuclear Physics, D-50937 Cologne, Germany*

(Dated: November 19, 2021)

**Background:** Superdeformed (SD) bands are suggested by theory around  $^{40}\text{Ca}$  and in lighter alpha-conjugate nuclei such as  $^{24}\text{Mg}$ ,  $^{28}\text{Si}$  and  $^{32}\text{S}$ . Such predictions originate from a number of theoretical models including mean-field models and antisymmetrised molecular dynamics (AMD) calculations. While SD bands have been identified in  $^{40}\text{Ca}$  and its near neighbours, evidence for their existence in the lighter, mid-shell nuclei is circumstantial at best. The key evidence for superdeformation would be observation of transitions with high  $B(E2)$  transition strengths connecting states in a rotational sequence. This is challenging information to obtain since the bands lie at high excitation energy and competition from out-of-band decay is dominant.

**Purpose:** The purpose of the present study is to establish a new methodology to circumvent the difficulties in identifying and quantifying in-band transitions through directly populating candidate states in the SD band in  $^{28}\text{Si}$  through inelastic alpha scattering, selecting such states with a spectrometer and measuring their gamma-ray decay with a large array of high-purity germanium detectors, allowing direct access to electromagnetic transition strengths.

**Methods:** Excited states in  $^{28}\text{Si}$  were populated in the  $^{28}\text{Si}(\alpha, \alpha')$  reaction using a 130-MeV  $^4\text{He}$  beam from the K140 AVF cyclotron at RCNP. Outgoing alpha particles were analysed using the Grand Raiden spectrometer positioned at an angle of  $9.1^\circ$  to favour population of states with  $J \approx 4$ . Coincident gamma rays were detected with the CAGRA array of twelve HPGe clover detectors augmented by a set of four large  $\text{LaBr}_3$  detectors.

**Results:** Data analysis showed that it was possible to identify additional low-energy transitions in competition with high-energy decays from excited states in  $^{28}\text{Si}$  in the vicinity of 10 MeV. However, while the candidate  $4^+$  SD state at 10.944 MeV was populated, a 1148-keV transition to the candidate  $2^+$  SD state at 9.796 MeV was not observed, and only an upper limit for its transition strength of  $B(E2) < 43$  W.u. could be established. This contradicts with AMD predictions of  $\sim 200$  W.u. for such a transition.

**Conclusion:** The present study strongly rejects the hypothesis that the candidate set of states identified in  $^{28}\text{Si}$  represent a superdeformed band, which demonstrates the potential of the methodology devised here.

## I. INTRODUCTION

Nuclear structure physics has historically categorised nuclei as spherical with associated vibrational spectra, and deformed with associated rotational spectra. Taking a global view of nuclear excited states, deforma-

---

\* david.jenkins@york.ac.uk

† Present address: Institute of Modern Physics, Chinese Academy of Sciences, Lanzhou 730000, China

tion and rotational excitation appears to be the model with the widest explanatory power. Indeed, even in the textbook examples of spherical nuclei, i.e. those with doubly-closed shells, deformation and rotational excitations are in evidence at low excitation energy heavily supporting a paradigm of shape coexistence [1]. Examples include the deformed band built on the first-excited  $0^+$  state in  $^{16}\text{O}$  and the superdeformed bands in  $^{40}\text{Ca}$  suggested to be associated with 4p-4h and 8p-8h excitations across the doubly-magic shell closure. The existence of the latter were first evidenced nearly 50 years ago in multi-alpha-particle transfer reactions [2] and later convincingly demonstrated through in-beam gamma-ray spectroscopy [3]. In these light alpha-conjugate systems, the origin of deformed and superdeformed structures has been described within various alpha-cluster models, e.g., antisymmetrized molecular dynamics (AMD) [4], within mean-field models [5] and within shell-model descriptions [6]. It is an open question whether these theories describe the same underlying physics and whether the additional degrees of freedom associated with alpha cluster models are essential to understand the associated nuclear structure.

Testing the models of shape coexistence in these light alpha-conjugate nuclei requires pushing down from  $^{40}\text{Ca}$  into the mid-shell region. A superdeformed band has been observed in an in-beam study of  $^{36}\text{Ar}$  [7] but the corresponding structures, which theoretical studies have predicted for  $^{24}\text{Mg}$  [8],  $^{28}\text{Si}$  [4] and  $^{32}\text{S}$  [5, 9, 10], have only limited experimental evidence in favour of their existence. For example, a recent internal pair measurement has determined  $\rho(E0)$  from the excited  $0^+$  state in  $^{24}\text{Mg}$  at 6.432 MeV to the ground state, which suggests that this state is bandhead of a highly-deformed band [11].

In this work, we focus on  $^{28}\text{Si}$  which has long been described as manifesting shape coexistence [12]. Prolate deformation is known to be the dominant form of deformation found in nuclei. By contrast,  $^{28}\text{Si}$  is one of the relatively few stable nuclei which has been shown to be oblate deformed in its ground state as evidenced by the deformed band built on the ground state and the positive sign of the quadrupole moment of the first-excited  $2^+$  state [13]. The ground-state band coexists with a prolate deformed band, well-studied in experiment, with a bandhead energy of 6691 keV. Narrow resonances have been observed in breakup reactions into  $^{12}\text{C}+^{16}\text{O}$  [14] as well as in radiative-capture cross sections [15, 16], which are suggested to correspond to  $^{12}\text{C}+^{16}\text{O}$  molecular states at high excitation energy in  $^{28}\text{Si}$ . This would correspond to a third co-existing structure of highly-deformed states that could be described as ‘‘hyper-deformed’’; such states play a potential role in  $^{12}\text{C}+^{16}\text{O}$  fusion in massive stars [17].

AMD calculations predict a rich pattern of rotational bands associated with  $^{28}\text{Si}$  [4, 18] based on  $^{24}\text{Mg}+\alpha$  and  $^{12}\text{C}+^{16}\text{O}$  cluster configurations. A search in the literature and recent experimental data in response to the AMD calculations for  $^{28}\text{Si}$  led to the identification of the

set of candidate SD states shown in Fig. 1 [19]. These comprise a rotational sequence with an implied moment of inertia matching the predictions of the AMD calculations for the SD band. Moreover, the transition strengths between this candidate band and the prolate deformed band are two orders of magnitude larger than the transition strengths to the corresponding states in the oblate ground-state band, suggesting some structural selectivity. Subsequent to the identification of these candidate SD states in  $^{28}\text{Si}$ , a study of the  $^{28}\text{Si}(\alpha,\alpha')$  reaction at very forward angles clearly identified the strong population of an additional  $0^+$  state at 9.71 MeV in  $^{28}\text{Si}$ . Such reactions are expected to strongly populate cluster states, and, therefore, while the excitation energy of this  $0^+$  state is not compatible with the 9.3 MeV expected from a smooth extrapolation of the candidate SD states, it has been suggested as the bandhead of the candidate superdeformed band based on its strong population in  $^{28}\text{Si}(\alpha,\alpha')$  and the absence of any other excited  $0^+$  states in the region from around 8.8 to 10 MeV [20].

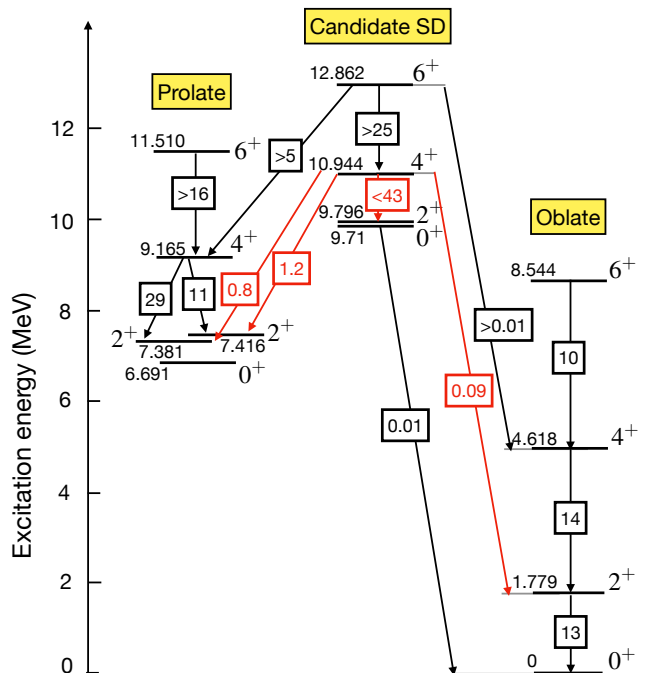


FIG. 1. Key elements of the band structure of  $^{28}\text{Si}$  relevant to the present work. The ground-state band is oblate deformed and co-exists with an excited prolate band. Candidate states for a superdeformed (SD) band are indicated. Transition strengths, i.e.  $B(E2)$  in W.u., are indicated where known, including limits. The transition strengths shown in red are those derived in the present work, as presented in Tab. I.

The key observable in support of assigning a superdeformed character to a rotational band would be the observation of strong  $B(E2)$  transitions connecting successive states in the candidate band. In the case of  $^{40}\text{Ca}$  and neighbouring isotopes, this has been readily achieved be-

cause the rotational bands lie close to the yrast line and are strongly populated in fusion-evaporation reactions. In the case of  $^{28}\text{Si}$ , the situation is much more challenging as the candidate band lies at high excitation energy and is far from being yrast. This implies that out-of-band transitions are high in energy and since transition rates for E2 transitions scale as  $E_\gamma^5$ , the decay branching of a superdeformed state would strongly favour the out-of-band decay. Moreover, the states of interest lie on or above the threshold for break-up into  $^{24}\text{Mg}+\alpha$  and so the gamma branch of these states may not necessarily dominate. In this sense, it is of high value to develop an experimental technique which can populate and select the state of interest and compare the relative intensities of the gamma-decay branches. If the population of the state in inelastic  $\alpha$  scattering is selected with a magnetic spectrometer then, in principle, comparing the efficiency-corrected gamma decay of this state to the population allows a correction to be made for the gamma branch.

Specifically, we seek to populate the  $4^+$  state at 10944 keV in the candidate superdeformed band of  $^{28}\text{Si}$  and establish a transition strength for the B(E2) transition to the candidate  $2^+$  state at 9796 keV, i.e. a transition energy of 1148 keV. If the candidate superdeformed band is correctly identified then this transition strength should be very large — predicted by AMD calculations to be around 200 W.u. [4]. Prior to the present study, the lifetime of the 10944 keV state was known but the gamma-branching of this state with respect to competing charged-particle breakup was not known.

## II. EXPERIMENT

Excited states in  $^{28}\text{Si}$  were populated using the  $^{28}\text{Si}(\alpha,\alpha')$  reaction using a 130-MeV  $^4\text{He}$  beam from the K140 AVF cyclotron at RCNP impinging on an 11- $\mu\text{m}$  thick ( $2.6\text{ mg/cm}^2$ )  $^{\text{nat}}\text{Si}$  target. The outgoing alpha particles were analysed using the Grand Raiden spectrometer. The spectrometer was positioned at an angle of  $9.1^\circ$  to favour population of states around  $J = 4$ . The focal plane of Grand Raiden comprised two multi-wire drift chambers, MWDC1 and MWDC2 followed by two plastic scintillator detectors, PS1 and PS2. Prompt gamma rays from the target position were recorded with the CAGRA array comprising twelve HPGe clover detectors and four large  $\text{LaBr}_3$  detectors. All but two of the clover detectors had BGO suppression shields. The  $\text{LaBr}_3$  detectors were mounted at forward angles ( $45^\circ$ ), while eight HPGe clovers were mounted at  $90^\circ$  and four at  $135^\circ$ . Shielding was applied to the front of the HPGe detectors to absorb X-rays and bremsstrahlung radiation comprising 2-mm of Pb and 2-mm of Cu. Given the forward focussing of intense scattered alpha particles and associated radiation, the  $\text{LaBr}_3$  detectors employed significantly thicker shielding, namely, 10-mm thickness of lead and 4-mm thickness of Cu.

Data from both Grand Raiden and the CAGRA ar-

ray were collected with a fully digital data-acquisition system, where the Grand Raiden readout was fully independent allowing focal-plane data to be separately analysed. A distributed timestamp allowed the data from the Grand Raiden focal plane and CAGRA array to be synchronised.

## III. DATA ANALYSIS

The Grand Raiden focal-plane data were analysed using the GR-analyzer framework developed at RCNP. Focal-plane data were corrected according to standard prescriptions, i.e. correcting particle ID gates for time-of-flight, and kinematic corrections to remove the scattering-angle dependence from the measured X position on the focal plane. The excitation energy resolution achievable was  $\approx 170$  keV (FWHM), of which  $\approx 70$  keV (FWHM) could be attributed to straggling in the target.

Data from the CAGRA array were processed using the GRUTinizer analysis framework developed at NSCL. The HPGe detectors were operating at a very high rate and significant efforts were needed in the data analysis to optimise their energy resolution. A detailed explanation and rationale for these corrections is provided in ref. [21]. Briefly, the focus of improvements was to the signal baseline, pole-zero correction and gain shifts. The signal baseline for the germanium detectors was found to oscillate strongly as a function of the detector rates, driven by the incident beam current, but was also observed to fluctuate on shorter time scales. This baseline oscillation on short time scales likely causes the most significant degradation in the germanium detector energy resolution that could be achieved; its origin is not completely clear but it may have arisen from electromagnetic interference originating from the accelerator. The issue with the baseline of the germanium detector signals was improved as far as possible by fitting the baseline with a moving average using the Kalman filter method. Due to the high rates, pulses in the germanium detector signal were frequently riding on the decaying tail of the previous pulse. This could be corrected by adjusting the pole zero parameter in the pulse-shape analysis routine. This was optimised to remove tails observed in the prominent 511 keV annihilation photopeak. The most severe impact of the high rates observed was a rate-dependent gain shift in the germanium spectra, which led to photopeaks appearing as multiple peaks. This was resolved by creating an algorithm which tracked the 511-keV peak centroid position. It was fitted every 30 seconds for every run and for each crystal. Each peak's measured centroid shift relative to 511 keV was tabulated. Then in the sorting process depending on the timestamp and crystal, the appropriate shift was applied. This method was found to be more robust than other methods explored, being more sensitive to discontinuities and large sudden changes in baseline. Following optimisation of the energy resolution for individual germanium crystals, a standard add-back methodology was

applied to the events in the HPGe clover detectors and BGO suppression was employed for the detectors with BGO shields. An event-by-event Doppler-shift correction was then applied using the kinematics of the  $^{28}\text{Si}$  recoil extracted from the alpha particle energy and angle as detected in the spectrometer focal plane. Sensitivity in the Doppler reconstruction was found for relatively long-lived states, e.g., 1 ps, for which the recoils largely stop in the target. Since the focus in this work was on unbound states with short half-lives  $\sim 10$  fs, the effects of the stopping process are largely unimportant.

#### IV. RESULTS

The calibrated focal-plane spectrum for Grand Raiden is presented in Fig. 2. The majority of the peaks identified in the focal-plane spectrum could be associated to well-known excited states in  $^{28}\text{Si}$  (see Fig. 3) while the remaining few are related to excited states in  $^{29}\text{Si}$  and  $^{30}\text{Si}$  due to their presence in the natural silicon target employed in the measurement. The majority of  $^{28}\text{Si}$  states excited are natural-parity states, which accords with the  $^{28}\text{Si}(\alpha, \alpha')$  reaction mechanism employed. A few unnatural-parity states such as the  $3^+$  state at 6276 keV are also excited, which must be due to a two-step reaction mechanism as both the beam and target are spin-0 bosons. The most strongly excited states in the focal-plane spectrum are the  $3^-$  and  $5^-$  states in the two ‘‘octupole’’ bands in  $^{28}\text{Si}$  (see Fig. 3). This appears to be in broad correspondence with the expectation that the angle range selected by the spectrometer would favour population of states with  $J \approx 4$ .

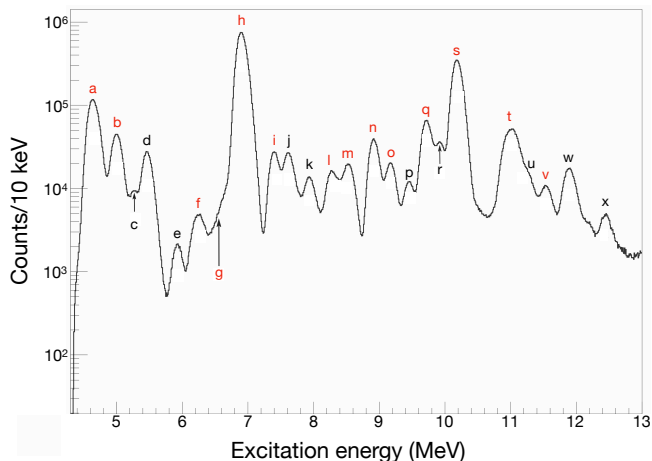


FIG. 2. Calibrated focal-plane spectrum. Peaks in the spectrum associated with population of known excited states in  $^{28,29,30}\text{Si}$  are identified with a letter. The peaks corresponding to excited states in rotational bands in  $^{28}\text{Si}$  are indicated in red (see Fig. 3).

#### A. Example analysis

Having identified the peaks in the focal-plane spectrum, it is now possible to create a matrix of gamma-ray events detected in prompt coincidence with population of a given state with a normalised random background subtraction applied (see Fig. 4). The detailed decay branching of a state can be examined by projecting a gamma-ray spectrum (or gamma-gamma matrix where statistics allow) from the coincidence data, gated on a given state.

Figure 5 presents an example of the analysis selecting events associated with population of the 6276-keV state in  $^{28}\text{Si}$ ; the expected transitions depopulating this level are clearly identified in the resulting spectrum. In addition, transitions associated with the decay of excited states in  $^{29}\text{Si}$  and  $^{30}\text{Si}$  are also observed. This is a consequence of the limited focal-plane energy resolution which makes it difficult in some cases to fully disentangle the population of multiple overlapping states in the focal-plane spectrum; this effect is also evident in the coincidence matrix presented in Fig. 4. In practice, the impact on the data analysis is low as the gamma-ray peaks due to the contaminant isotopes are well known and well separated in energy from the transitions of interest in  $^{28}\text{Si}$ .

#### B. Demonstration of ability to find new transitions

Critical to the present work is the ability to discriminate previously unobserved low-energy gamma rays in competition with high-energy transitions. In some cases, the present data analysis has allowed this to be achieved. Figure 6 presents an example with the low-energy portion of the gamma-ray spectrum for events associated with the doublet of states at 10182 keV ( $3^-$ ) and 10190 keV ( $5^-$ ) in the Grand Raiden focal-plane spectrum. Two previously unobserved low-energy gamma-ray transitions are identified in this spectrum with energies of 799.5 and 865.4 keV. These would correspond to transitions from the  $3^-$  state at 10182 keV to the  $2_6^+$  state at 9382 keV and to the  $3_4^+$  state at 9316 keV, respectively; both transitions would accordingly have E1 multipolarity.

#### C. Candidate SD transition

Having verified that identifying low-energy peaks is possible, we turn our attention to the principal focus of this study: searching for a 1148 keV transition from the 10944 keV ( $4_7^+$ ) state to the 9796 keV ( $2_{10}^+$ ) state in the candidate superdeformed band. Given the overlapping peaks in the focal-plane spectrum and the limited energy resolution, a gate on the 10944 keV ( $4_7^+$ ) state in the focal plane appears to select at least two other states: the 11079 keV ( $3_6^-$ ) state and a further state at 11012 keV, whose assignment we discuss below. Figure 7 presents the high-energy portion of the gamma-ray spectrum in coincidence with the focal-plane selection. In this spectrum,

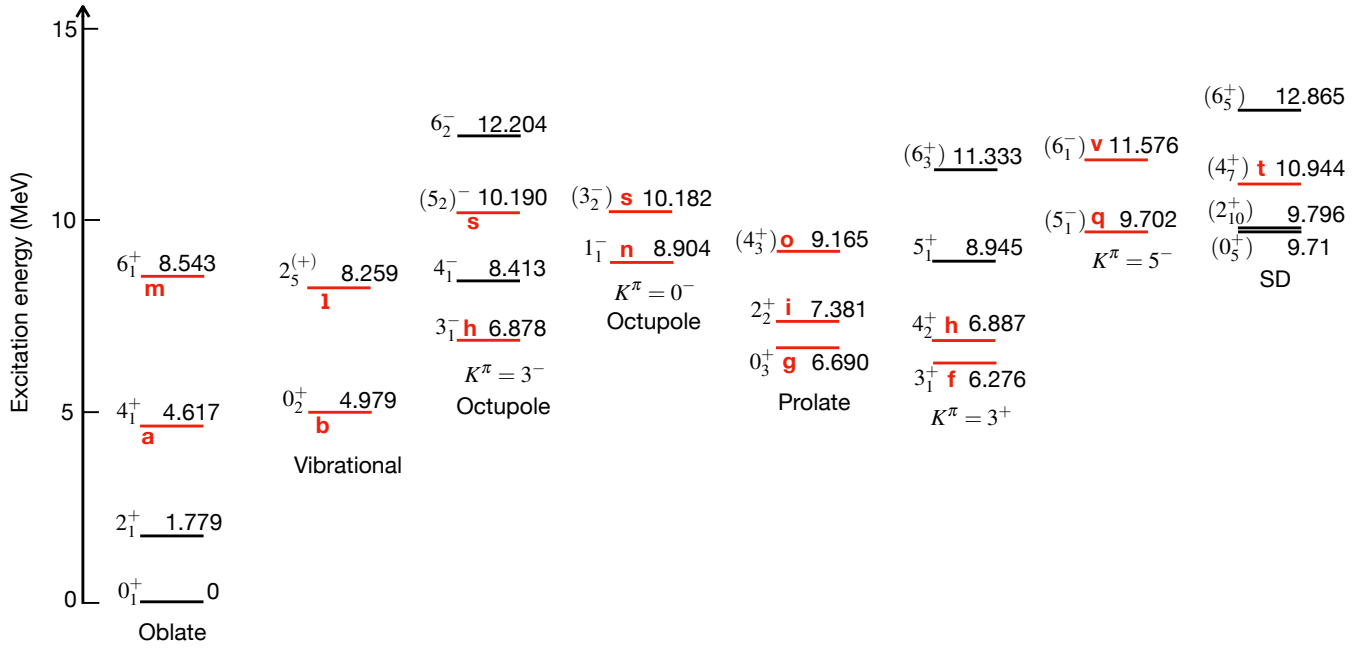


FIG. 3. Subset of the excited states and rotational bands in  $^{28}\text{Si}$ . The rotational bands are labelled with the  $K^\pi$  assigned to them in the literature. The rotational sequence labelled as “SD” is the candidate superdeformed band. Those states marked in red were populated in the present study; they are labelled with a letter which corresponds with the peaks observed in the focal-plane spectrum (see Fig. 2).

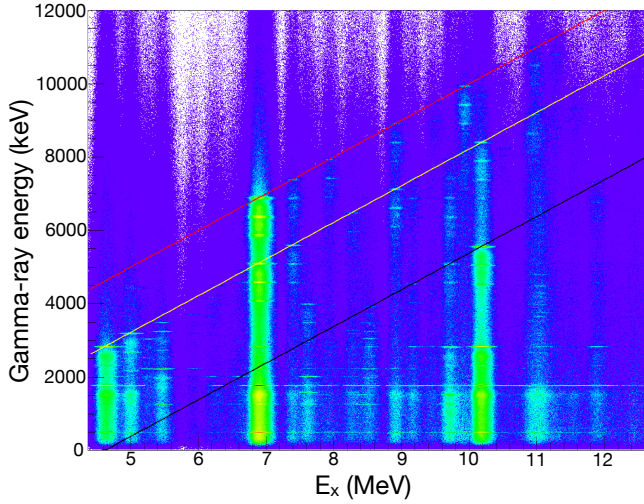


FIG. 4. Background-subtracted coincidence matrix of gamma-rays in prompt coincidence with detection of alpha particles at the focal plane corresponding to population of excited states in  $^{28}\text{Si}$ . The red line indicates the locus corresponding to transitions to the ground state, the yellow to the  $2_1^+$  state and black to the  $4_1^+$  state in  $^{28}\text{Si}$ .

high-energy ( $\sim 9$  MeV) transitions from the  $4_7^+$  and  $3_6^-$  states to the  $2_1^+$  state, with their associated escape peaks, are clearly observed. A transition (with associated escape peaks) is observed at 11007 keV, which must be a direct decay to the ground state. Taking account of the nuclear

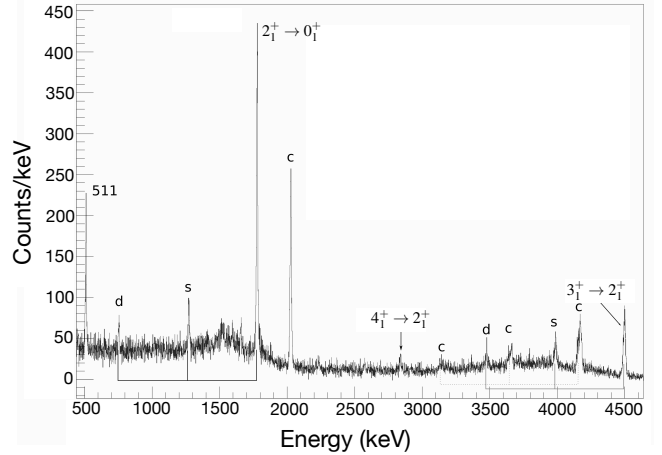


FIG. 5. Sample gamma-ray spectrum obtained by gating on the  $3_1^+$  state at 6276 keV in the focal-plane data. Single- and double-escape peaks are marked ‘s’ and ‘d’, respectively. Contaminant peaks from other silicon isotopes,  $^{29}\text{Si}$  and  $^{30}\text{Si}$  are marked with ‘c’.

recoil correction for such a high energy gamma-ray (4.6 keV), this would imply the existence of a narrow 11012-keV state with possible  $J^\pi = 1^-, 1^+$  or  $2^+$ . We note that, given the transition energy is so high, and so far outside the range of the standard calibration carried out with a  $^{56}\text{Co}$  source, a systematic deviation is possible. In this case, the 11012 keV state, whose excitation energy is extracted solely from its gamma decay, could correspond

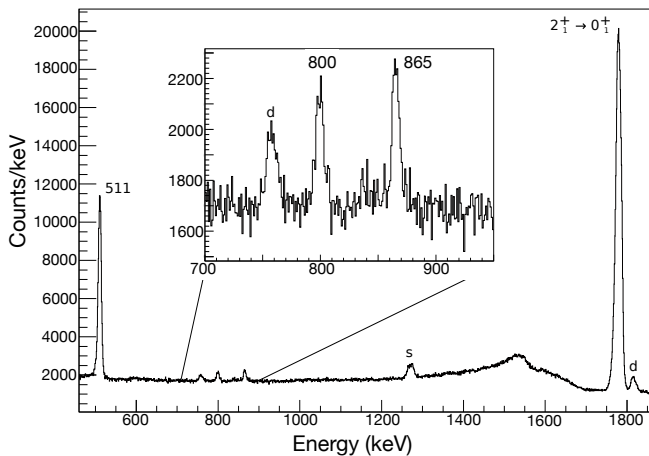


FIG. 6. Gamma-ray spectrum obtained by gating on the 10182/10190 keV doublet. Peaks marked ‘s’ and ‘d’ are single- and double-escape peaks, respectively. The inset shows an expanded view of the gamma-ray spectrum between 700 and 950 keV where two new transitions with energies of  $\sim 800$  and  $\sim 865$  keV are identified.

to the  $1^-$  state at 10994(2) keV, previously observed in several different studies, and which was shown to have an 85 % gamma-decay branch to the ground state [22].

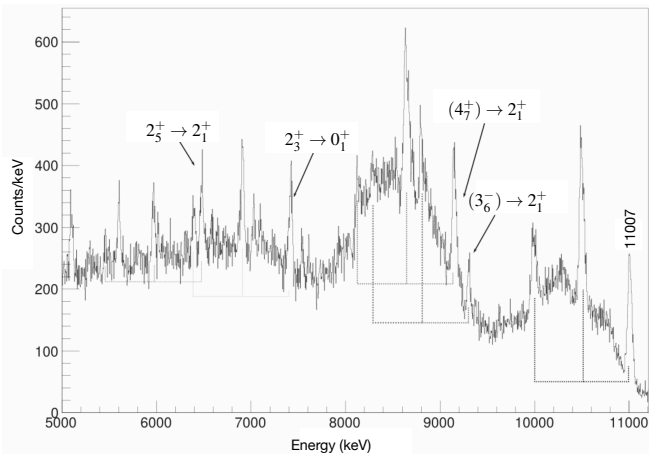


FIG. 7. High-energy portion of gamma-ray spectrum gated by the 10944 keV state. Each transition is labelled and the position of single- and double-escape peaks with respect to the photopeak is indicated with the dotted lines. A previously unreported transition with an energy of 11007 keV is marked.

Figure 8 presents the coincident gamma-ray spectrum in the energy range 2 - 5 MeV. In this spectrum, additional known decay branches of the 10944 keV state are observed including the 2685 keV ( $4_7^+ \rightarrow 2_5^+$ ), 3527 keV ( $4_7^+ \rightarrow 2_3^+$ ) and 3563 keV ( $4_7^+ \rightarrow 2_2^+$ ) transitions. This gives further confidence that the correct state is selected at the focal plane and that the coincidence analysis is functioning well. As noted in the caption to Fig. 8, a single peak associated with  $^{30}\text{Si}$  is observed in this spectrum, reflecting the difficulty in fully separating excited

states in the focal-plane spectrum given the focal-plane energy resolution.

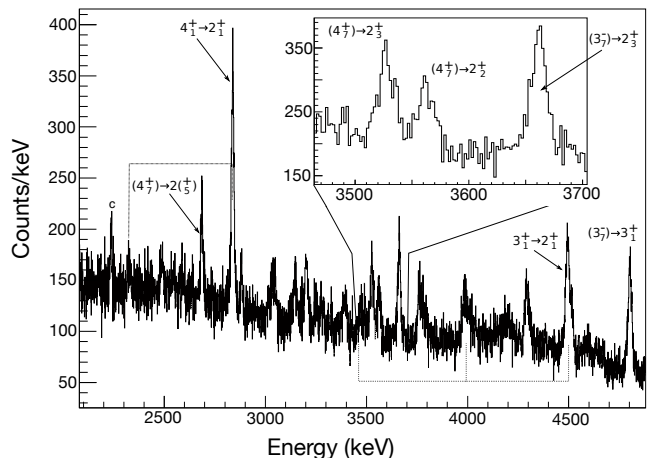


FIG. 8. Mid-energy portion of gamma-ray spectrum gated by the 10944-keV state. Transitions are labelled and the location of single- and double-escape peaks relative to the photopeak is indicated with the dotted lines. The inset shows an expanded view of the region between 3500 and 3700 keV where three transitions of interest are located. For reasons of clarity, only the key transitions relevant to the present analysis are marked. The remaining peaks are all associated with known transitions in  $^{28}\text{Si}$  with the exception of the peak labelled ‘c’ which is a known transition in  $^{30}\text{Si}$  associated with weak selection of the state labelled ‘u’ in Fig. 3 which sits on the shoulder of the state of interest, ‘t’.

Figure 9 presents the low-energy portion of the spectrum where the 1148 keV transition should appear. There are only three identifiable features in this spectrum: the Compton background and single-escape peak associated with the 1778  $2_1^+ \rightarrow 0_1^+$  transition, and the previously known 1697 keV transition ( $(3_6^-) \rightarrow 2_6^+$ ). It is therefore only practical to obtain an upper limit for the intensity of the unobserved 1148 keV transition. This was achieved by fitting a Gaussian peak to the spectrum with a fixed centroid energy of 1148 keV and a FWHM for the peak fitting fixed as 6.93 keV; this FWHM was obtained by parameterising the observed FWHM of gamma-ray peaks observed under different gating conditions. The result of the fit yielded  $60 \pm 64$  counts above background, i.e. consistent with zero.

#### D. Gamma branching and transitions strengths of decays from 10.944-MeV state

In principle, it would be possible to correct for the unseen particle branch of states above the particle-decay thresholds by comparing the sum of the intensity of gamma rays directly de-exciting the state of interest to the population of state observed in Grand Raiden when account is taken of the relevant efficiencies. This was not practical for the 10.944 MeV state because of the

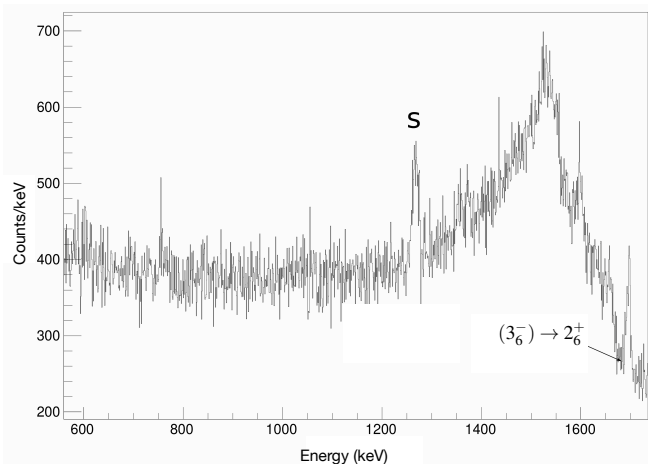


FIG. 9. Low-energy portion of gamma-ray spectrum gated by the 10944 keV state. The single-escape peak corresponding to the intense 1778 keV  $2^+ \rightarrow 0^+$  transition is marked with 's' and the  $(3_6^-) \rightarrow 2_6^+$  transition is labelled.

fact that several states were found to be overlapping given the effective Grand Raiden excitation energy resolution. However, the only allowed particle decay of the 10.944 MeV state would be emission of an  $L = 4$  alpha particle. The Wigner limit for such a decay corresponds to  $1.94 \times 10^{-6}$  eV, or a partial half-life of 0.34 ns. Given the measured half-life of the 10.944 MeV state is 15(10) fs [23], it is safe to treat this state as effectively 100 % gamma-decaying.

Using the partial half-life for the 10.944-MeV state and the gamma branchings of the state derived from the present work,  $B(E2)$  transition strengths may be evaluated. Since there is a large uncertainty in the partial half-life, it is not appropriate to use standard error propagation and, therefore, a Monte-Carlo method was used to obtain the respective errors. The results of this analysis are tabulated in Tab. I. Since the 1148 keV transition could not be identified above background, it is more appropriate to consider the transition strength obtained for it as an upper limit, i.e.  $B(E2) < 43$  W.u. considering the minimum and maximum of each variable used in its derivation. The uncertainties in the  $B(E2)$  transition strengths are dominated by the precision in knowledge of the half-life of the 10.944 MeV state. Strictly speaking, there will be an additional systematic error in these results as the gamma branching did not take into account the angular distributions of the gamma rays which was impractical given the low statistics and limited set of detector angles. However, this effect should be minimal as all transitions have E2 multipolarity and should be to first order, very similar.

Transition	Energy (keV)	Branching ratio (%)	$B(E2)$ (W.u.)
$(4_7^+) \rightarrow 2_1^+$	9162	78.3(24)	$0.09^{+0.1}_{-0.04}$
$(4_7^+) \rightarrow 2_2^+$	3563	6.0(2)	$0.8^{+0.9}_{-0.3}$
$(4_7^+) \rightarrow 2_3^+$	3527	8.5(3)	$1.2^{+1.2}_{-0.5}$
$(4_7^+) \rightarrow 2_5^+$	2685	7.0(3)	$3.7^{+4.2}_{-1.6}$
$(4_7^+) \rightarrow (2_{10}^+)$	1148	0.18(19)	$7^{+36}_{-7}$

TABLE I. Gamma-ray decays of the 10.944 MeV state: transition, transition energy, branching ratios normalised to 100 % and the corresponding  $B(E2)$  transition strength in Weisskopf units.

## V. CONCLUSIONS

A search was carried out for the  $4^+ \rightarrow 2^+$  transition within a candidate superdeformed band in  $^{28}\text{Si}$ . The present study did not have sufficient sensitivity to identify such a transition and only an upper limit could be assigned to its transition strength corresponding to  $B(E2) < 43$  W.u. Nevertheless, this upper limit is five times less than AMD model predictions for the transition strength for such a  $4^+ \rightarrow 2^+$  transition in the superdeformed band. This study therefore strongly rejects the hypothesis that the set of candidate states identified represent the superdeformed band predicted by AMD calculations. Indeed, the previous experimental evidence for the superdeformed band in  $^{28}\text{Si}$  was circumstantial and based on observation of an  $I(I+1)$  sequence of states with an implied moment-of-inertia matching the AMD calculations. This re-emphasises the difficulties in experimentally locating superdeformed bands in such light nuclei given their high excitation energy. This study has proven an effective demonstration of the potential of the technique devised here, namely to search for low intensity in-band transitions in competition with dominant out-of-band decay. The major challenge found in the present study was in the quality of germanium detector spectra and degradation in energy resolution due to the high counting rates and short time scale oscillations in the signal baseline. Future improvements in these experimental aspects would allow such studies to be carried out in a more sensitive fashion.

## VI. ACKNOWLEDGEMENTS

This work was supported by the International Joint Research Promotion Program of Osaka University and by the Deutsche Forschungsgemeinschaft (DFG) under Grant No. SFB 1245, project ID 279384907. The Nuclear Data Review Group from NNDC, Brookhaven National Laboratory is acknowledged for their advice in handling presentation of  $B(E2)$  limits and their extraction using Monte-Carlo techniques for variables with large uncertainties.

- 
- [1] K. Heyde and J. Wood, *Rev. Mod. Phys.* **83**, 1467 (2011).
- [2] R. Middleton, J. Garrett, and H. Fortune, *Phys. Lett. B* **39**, 339 (1972).
- [3] E. Ideguchi *et al.*, *Phys. Rev. Lett.* **87**, 222501 (2001).
- [4] Y. Taniguchi, Y. K. En'yo, and M. Kimura, *Phys. Rev. C* **80**, 044316 (2009).
- [5] H. Molique, J. Dobaczewski, and J. Dudek, *Phys. Rev. C* **61**, 044304 (2000).
- [6] E. Caurier, J. Menendez, F. Nowacki, and A. Poves, *Phys. Rev. C* **75**, 054317 (2007).
- [7] C. Svensson *et al.*, *Phys. Rev. Lett.* **85**, 2693 (2000).
- [8] M. Freer, *Rep. Prog. Phys.* **70**, 2149 (2007).
- [9] R. Rodríguez-Guzmán, J. Egido, and L. Robledo, *Phys. Rev. C* **62**, 054308 (2000).
- [10] M. Kimura and H. Horiuchi, *Phys. Rev. C* **69**, 051304 (2004).
- [11] J. Dowie *et al.*, *Phys. Lett. B* **811**, 135855 (2020).
- [12] I. Ragnarsson and S. Åberg, *Phys. Lett. B* **114**, 387 (1982).
- [13] D. Pelte, O. Häusser, T. Alexander, B. Hooton, and H. Evans, *Phys. Lett. B* **29**, 660 (1969).
- [14] N. Ashwood, J. Murgatroyd, N. Clarke, M. Freer, B. Fulton, A. S. J. Murphy, S. Chappell, R. Cowin, G. Dillon, D. Watson, W. Catford, N. Curtis, M. Shawcross, and V. Pucknell, *Phys. Rev. C* **63**, 034315 (2001).
- [15] D. Lebhertz *et al.*, *Phys. Rev. C* **85**, 034333 (2012).
- [16] A. Goasduff, S. Courtin, F. Haas, D. Lebhertz, D. Jenkins, J. Fallis, C. Ruiz, D. Hutcheon, P.-A. Amandruz, C. Davis, U. Hager, D. Ottewell, and G. Ruprecht, *Phys. Rev. C* **89**, 014305 (2014).
- [17] X. Fang *et al.*, *Phys. Rev. C* **96**, 045804 (2017).
- [18] Y. Taniguchi and M. Kimura, *Phys. Lett. B* **800**, 135086 (2020).
- [19] D. Jenkins *et al.*, *Phys. Rev. C* **86**, 064308 (2012).
- [20] P. Adsley *et al.*, *Phys. Rev. C* **95**, 024319 (2017).
- [21] L. Morris, *Electromagnetic transitions as a probe for Superdeformation in  $^{28}\text{Si}$*  <https://etheses.whiterose.ac.uk/27271/>, Ph.D. thesis, University of York (2020).
- [22] E. Strandberg *et al.*, *Phys. Rev. C* **77**, 055801 (2008).
- [23] P. Endt, C. Alderliesten, F. Zijderhand, A. Wolters, and A. V. Hees, *Nucl. Phys. A* **510**, 209 (1990).